On the Control Bandwidth of Servo Drives

Joachim Böcker[1], Stephan Beineke[2], Alexander Bähr[2]
[1] Paderborn University, Power Electronics and Electric Drives, Paderborn, Germany
[2] LTi DRiVES GmbH, Lahnau, Germany
E-Mail: [1] boecker@lea.upb.de; [2] stephan.beineke@lt-i.com
URL: [1] http://wwwlea.upb.de; [2] http://www.lt-i.com

Keywords

«Control bandwidth», «control of drive», «converter control», «servo-drive», «current control», «torque control», «speed control»

Abstract

In this paper, the control performance of servo drives is being investigated. In this context, particular focus is put on the achievable control bandwidth, dependant on the chosen design parameters such as sampling rate, sampling strategy, and filter constants.

1 Introduction

The quality of servo drives is usually characterized by performance parameters like rise time, bandwidth, or controller sampling time. However, as common standards do not exist, it is difficult to compare those parameters between various suppliers. Thus, the intention of this paper is to review the basic control design rules, to show the interrelationship between control specifications, and to point out the general limits of control designs, particularly with respect to the achievable bandwidth.

The paper focuses on a cascaded control structure as shown in Fig. 1, which is widely spread in today's servo drive controls. The structure consists of an inner current or torque control loop and outer speed and position control loops. All controllers are assumed to have *PI* characteristics, as usually reverted to in this field of application.

2 Torque and Current Control

In flux-oriented controls of three-phase motors, the torque control aims at controlling the torque generating current component. Therefore, rotational transformations, decoupling, and an EMF feedforward compensation are applied. This paper shall refrain from describing the previously mentioned steps as they have already been discussed in a variety of textbooks, e.g. [1], [2]. The remaining "plant" can be considered as a PT_1 delay system with stator time constant $\tau_s = R_s / L_s$. Further delays and dead times in the control loop are caused by sensors, analogue filtering, sample-hold elements, and the computational delay of digital control. Despite the fact that delay and dead time cause different dynamical effects, the sum of all these effects can be described with a total dead time $T_{\Sigma,I}$. The dynamical behaviour of the plant is comprised in the transfer function

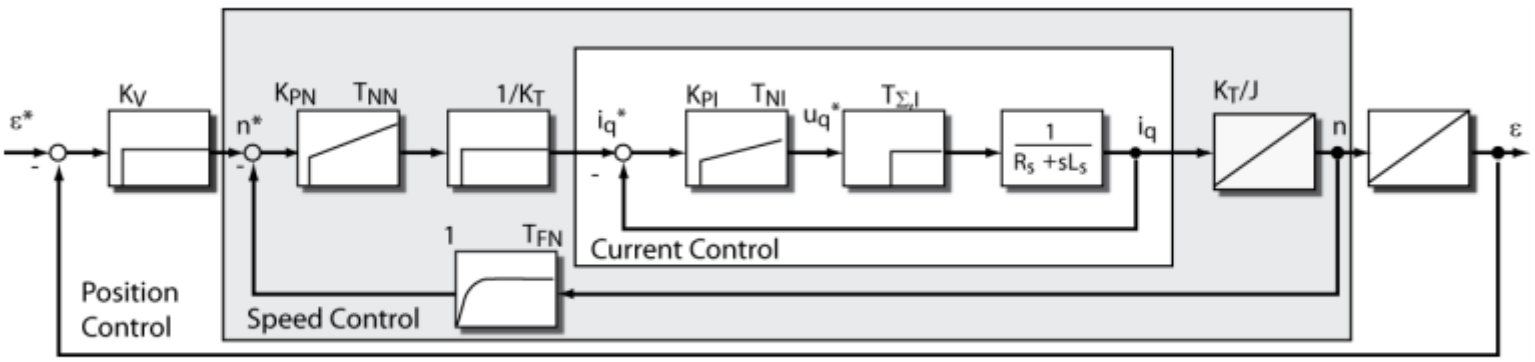

Fig. 1: Cascaded servo control structure

$$G_{PI}(s) = \frac{1}{R_s + sL_s} e^{-sT_{\Sigma,I}} \quad . \tag{1}$$

Alternatively, the plant transfer function can be regarded as a PT_2 delay system

$$G_{PI}(s) = \frac{1}{(R_s + sL_s)(1 + sT_{\Sigma,I})} \quad . \tag{2}$$

A measurement-based model validation (cp. Fig. 4) will, however, show that the approximation of the actual plant via Eq. (1) using a dead time, is more realistic than the PT_2 system in Eq. (2) relying on delay times, exclusively. Therefore, we will proceed with our first assumption in the following.

For current control, *PI*-compensators

$$G_{CI}(s) = K_{PI}\left(1 + \frac{1}{sT_{NI}}\right) \tag{3}$$

are commonly preferred, as the differential action of *PID* controllers introduce too much noise in the control loop. As a common design rule, the controller reset time is set to $T_{NI} = \tau_s$. This approach is known as open-loop shaping and leads to a pole-zero-cancellation in the open-loop and reference transfer functions. This cancellation does not occur in the disturbance transfer function, however. Introducing the normalized controller gain

$$\gamma = \frac{K_{PI} T_{\Sigma,I}}{L_s} \tag{4}$$

and the normalized frequency

$$\Omega = \omega T_{\Sigma,I}, \tag{5}$$

the open-loop and reference transfer functions F_{OI} and F_{WI} result to

$$F_{OI}(j\Omega) = G_{PI}(j\Omega) G_{CI}(j\Omega) = \gamma \frac{e^{-j\Omega}}{j\Omega} \quad , \tag{6}$$

$$F_{WI}(j\Omega) = \frac{F_{OI}(j\Omega)}{1 + F_{OI}(j\Omega)} = \frac{\gamma}{\gamma + j\Omega\, e^{j\Omega}} = \frac{\gamma}{\gamma - \Omega \sin\Omega + j\Omega\cos\Omega} \quad . \tag{7}$$

The loop shaping design provides a phase margin of

$$\phi_R = 90° - \frac{180°}{\pi}\gamma \quad . \tag{8}$$

As a compromise between sufficient damping on the one hand and a dynamic response on the other hand, $\gamma = 1/2$, known as the Magnitude Optimum, is often chosen as controller gain, resulting in a phase margin of 61°. Other values with $\gamma \le 1$ are also applied in practice.

If the assumption of a dead time is replaced by a delay with time constant $T_{\Sigma,I}$ according to Eq. (2), open-loop and reference transfer function would result as

$$F_{OI}(j\Omega) = \frac{\gamma}{j\Omega - \Omega^2} \quad , \quad F_{WI} = \frac{\gamma}{\gamma + j\Omega - \Omega^2} \quad . \tag{9}$$

3 Current Control Bandwidth

The bandwidth Ω_{BA} of a transfer system is defined as the frequency, at which the magnitude is attenuated by a factor of $1/\sqrt{2}$, i.e. by 3 dB. The phase shift, which is crucial for the control design, is, however, not considered in this definition. Therefore, an alternative bandwidth $\Omega_{B\phi}$ at which the

phase shift exceeds 90° shall be introduced. The relationships between normalized controller gain γ and the bandwidths Ω_{BA} and $\Omega_{B\phi}$ can easily be derived from (7) as

$$\gamma = \Omega_{BA}\left(\sqrt{\sin^2 \Omega_{BA} + 1} - \sin \Omega_{BA}\right) \tag{10}$$

and

$$\gamma = \Omega_{B\phi} \sin \Omega_{B\phi} \quad . \tag{11}$$

As depicted in Fig. 2, the phase condition is usually more restrictive than the magnitude condition. Only for small gains $\gamma < \sin^{-1}(1/\sqrt{3})/\sqrt{3} = 0.355$, the magnitude bandwidth determines the lower margin. With the standard design of $\gamma = 1/2$, the normalized bandwidth calculates to $\Omega_{B\phi} = 0.74$ or

$$f_{B\phi} = \frac{\Omega_{B\phi}}{2\pi T_{\Sigma,I}} \approx \frac{0.12}{T_{\Sigma,I}} \quad . \tag{12}$$

With higher controller gain, the bandwidth can be increased up to $\Omega_{B\phi} \approx 1$ or even a bit higher, resulting in smaller phase margins and thus poor damping characteristics, however. Therefore, the best way in order to gain high bandwidths is to decrease $T_{\Sigma,I}$.

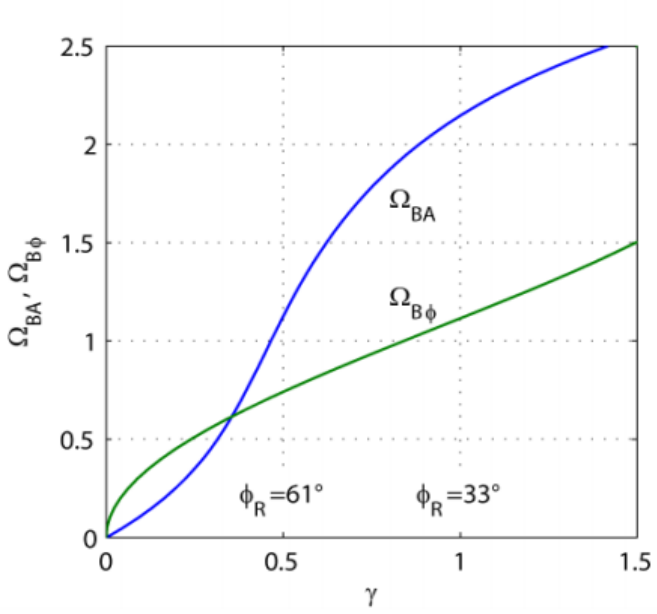

Fig. 2: Normalized current control bandwidths vs. controller gain γ

Whether Ω_{BA} or $\Omega_{B\phi}$ is more relevant, depends on the specification of the application. E. g. for tracking control in multi-axle machine tools, it is most important to follow a given track without spatial deviation, whereas following the track without time delay is not that relevant. In this case, the tracking behaviour is characterized by the magnitude bandwidth on the additional condition that the group delay time should be constant and equal for all axles, i.e. the phase shift should increase linearly with the frequency.

4 Sampling Strategy

The main portion of $T_{\Sigma,I}$ is usually contributed by the computational delay and measurement sampling. With the control sampling time T_c and the assumption that the Regular Sampling approach is applied (cp. Fig. 3, cases a and c), the effective dead time results in $T_{\Sigma,I} \approx 1.5\, T_c$. A portion of $1 \cdot T_c$ is caused by the computational delay of the control algorithm, another portion of $T_c/2$ can be ascribed to the sample/hold mechanism. Although, the exact transfer function of a sample/hold

element is known as $(1-e^{-sT_c})/sT_c$, it can be approximated quite accurately by $e^{-sT_c/2}$, i.e. a dead time of $T_c/2$.

If the controller is implemented on a fast responding field programmable gate array (FPGA) instead of a sequentially working processor, the computational delay can be neglected (case d), leading to $T_{\Sigma,I} \approx 0.5\,T_s$. The effective dead time can be reduced even more with the help of oversampling, i.e. if sampling, control, and updating of the PWM reference is conducted several times within one switching period. The oversampling rate of only 2 in case c can be increased even further in this context.

These various sampling strategies clearly reveal that the control performance can neither be accurately assessed by the switching frequency $f_s = 1/T_s$, which is equal in all considered cases, nor by the sampling frequency $f_c = 1/T_c$, in case the particular timing strategy is not disclosed.

For example, a typical switching frequency of f_s = 16 kHz leads to a dead time of $T_{\Sigma,I} = 93.75\,\mu s$ in case a, while the timing strategy used in case b can realize dead times of only $T_{\Sigma,I} = 62.5\,\mu s$. In the latter case, the characteristic bandwidths lie around $f_{B\phi} \approx 1.9\,kHz$ and $f_{BA} \approx 2.8$ kHz, respectively, assuming a gain of $\gamma = 0.5$.

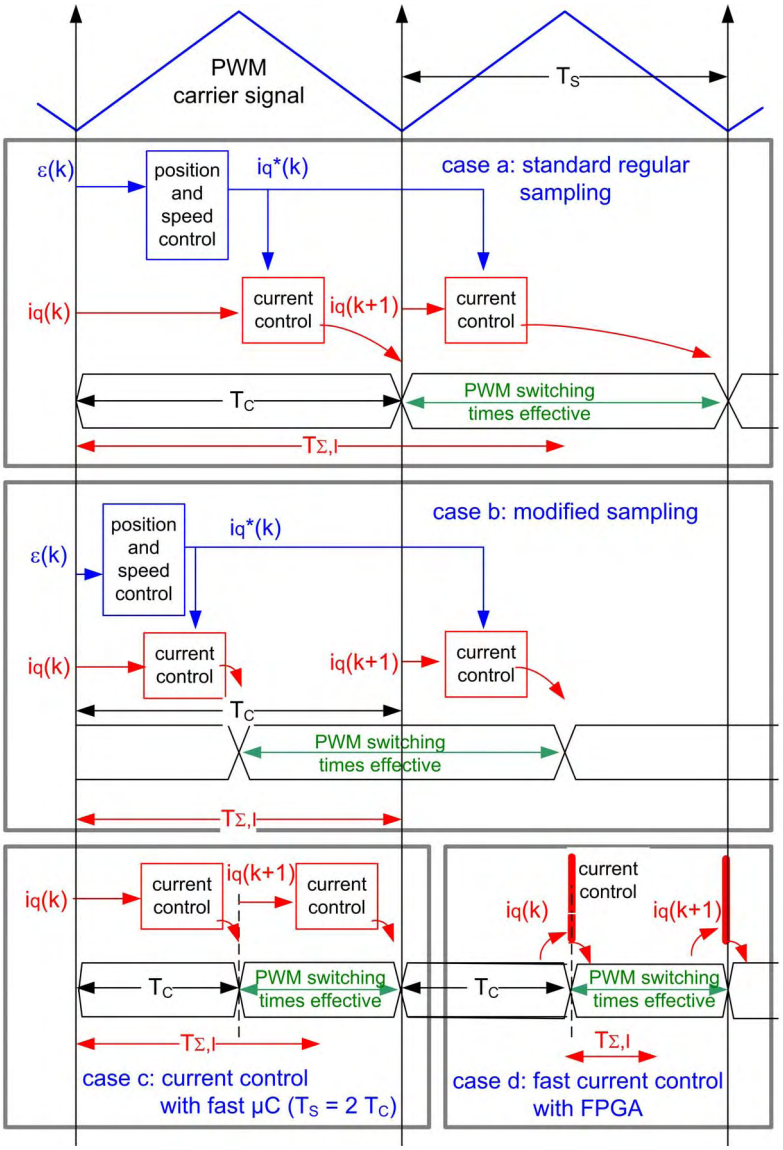

Fig. 3: Gantt diagrams of control processing task timing with different sampling strategies

For this configuration, measured and calculated frequency responses are compared in Fig. 4. All measurement data were taken from a linear ironless motor drive, which is used in applications where highest dynamics are required, e.g. fast tools servos, pick and place procedures, or bonding machines. The motor features low electrical and mechanical time constants and is fed by the *ServoOne* inverter from the company LTi Drives. *ServoOne* relies on the optimized sampling scheme in case b of Fig. 3. In Fig. 4 it can be seen that the frequency response, resulting from the assumption of an effective dead time in the current loop (cp. Eq. (1)), approximates the measurement quite well (dark green curves). In contrast, an assumed PT_2 delay behaviour of the open loop, as proposed by Eq. (2) provides less accurate results (blue curves). Furthermore, it can be seen from the red curves, that a delay approximation of the closed-loop transfer function

$$F_{WI}(s) \approx \frac{1}{1+sT_{EI}} \quad \text{with} \quad T_{EI} = \frac{T_{\Sigma,I}}{\gamma} \tag{13}$$

is, though often applied, not very accurate and requires at least a critical analysis of its extent of validity (corresponding corner frequencies $f_{EI} = 1/2\pi T_{EI}$ are marked with red dots).

Fig. 5 shows measurements of step responses for different controller gains γ. While $\gamma = 1$ leads to a quite short rise time, the amplitude of the overshoot is not acceptable. That is why controller gains γ are usually set to values within the range of 0.5 to 0.8. The measurement data has been acquired by the data recording system of the *ServoOne* inverter and can only be provided at the sampling instants.

a) $\gamma = 0.5$

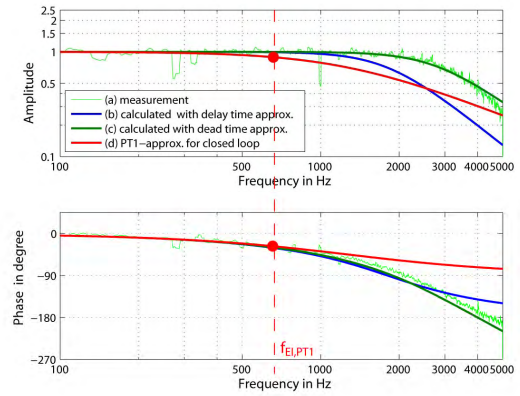

b) $\gamma = 0.78$

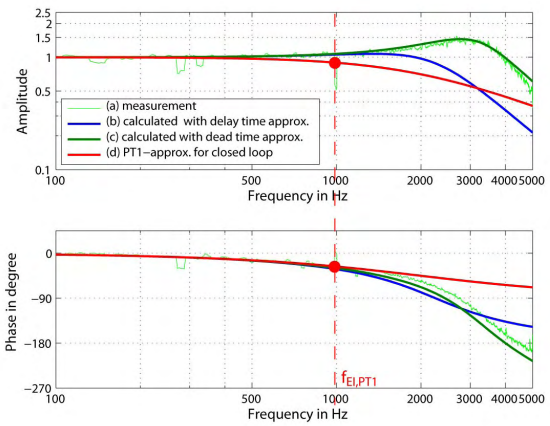

c) $\gamma = 0.78$

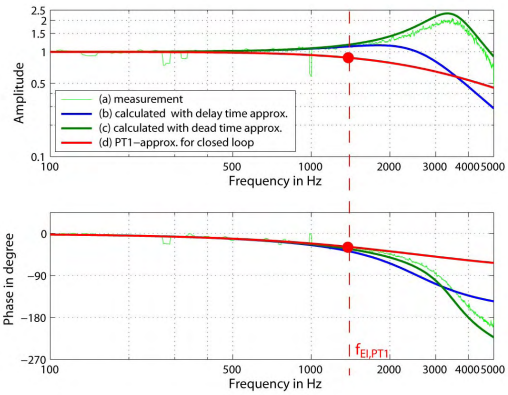

Fig. 4: Current control reference transfer frequency responses (calculations compared with measurement)

a) $\gamma = 0.5$

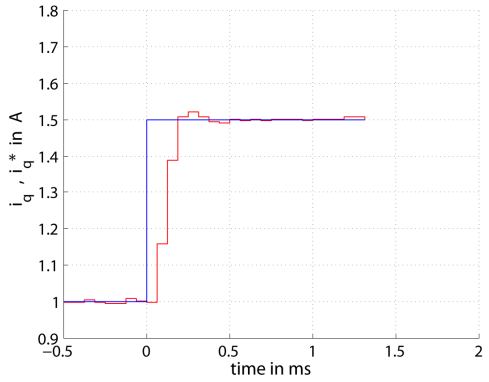

b) $\gamma = 0.78$

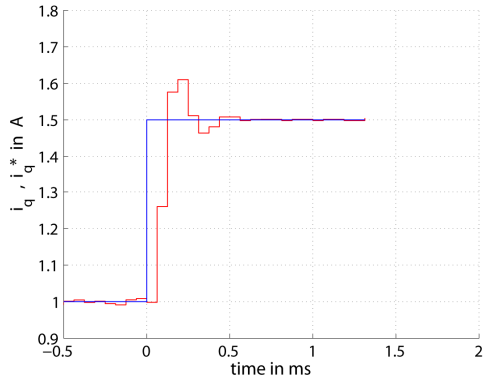

c) $\gamma = 1$

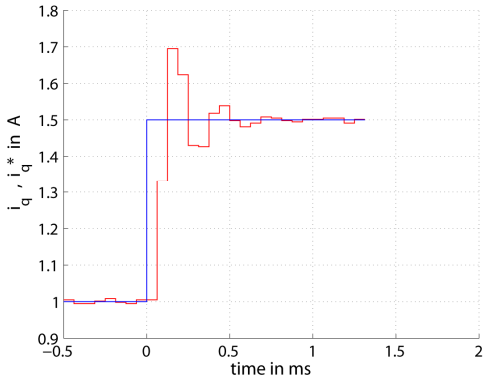

Fig. 5: Measurements of current control reference step responses

5 Speed Control

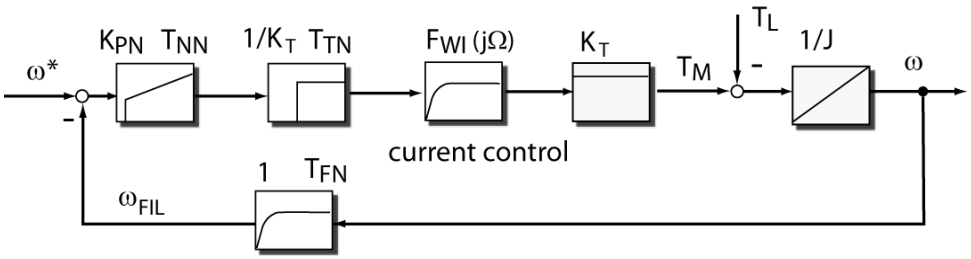

Fig. 6: Speed control loop

For the design of the speed control, it is assumed that the behaviour of the mechanical subsystem can be described as inertia J resulting in an integrator. A speed filter is usually required in order to smooth the speed signal and to suppress the artefacts of the sensor, e.g. of the incremental decoders, see Fig. 6. The speed filter is represented by a first-order delay with time constant T_{FN}. The speed control algorithm will usually cause additional computational delays T_{TN}. The behaviour of the inner torque generating current control is represented by the reference transfer function F_{WI}. The motor constant K_T is directly compensated by an appropriate controller gain, resulting in the open-loop and closed-loop speed control transfer functions

$$F_{ON}(s) = K_{PN}\left(1+\frac{1}{sT_{NN}}\right)\frac{1}{sJ}F_{WI}(s)\frac{e^{-sT_{TN}}}{1+sT_{FN}}\ , \tag{14}$$

$$F_{WN}(s) = \frac{F_{ON}(s)}{1+F_{ON}(s)}\ . \tag{15}$$

The task is now to design a speed controller, assuming again *PI* characteristics, with gain K_{PN} and reset time T_{NN}. In this context, a reasonable trade-off between dynamic control response and smooth stationary operation without oscillations or audible noise must be found. A suitable controller design method for target plants with integrators is the Symmetrical Optimum. To apply this method, all dead and delay times of the speed control loop are merged into one single effective delay time

$$T_{\Sigma,N} = T_{EI} + T_{FN} + T_{TN} \ . \tag{16}$$

That included the approximation of the current transfer behaviour according to Eq. (13) though this approximation has only restricted accuracy as discussed above. We will come back to this point below. With that assumption, the open-loop transfer function is simplified to

$$F_{ON}(s) \approx K_{PN}\left(1+\frac{1}{sT_{NN}}\right)\frac{1}{sJ}\,\frac{1}{1+sT_{\Sigma,N}} = \frac{K_{PN}\left(1+sT_{NN}\right)}{s^2 JT_{NN}\left(1+sT_{\Sigma,N}\right)} \ . \tag{17}$$

According to the design rules of the Symmetrical Optimum method [2], the controller parameters are set to

$$T_{NN} = \alpha^2\, T_{\Sigma,N} \ , \quad K_{PN} = \frac{J}{\alpha\, T_{\Sigma,N}} \tag{18}$$

with a free design parameter α that typically lies within the range of 2 to 4. The gain crossover frequency now results in

$$\omega_{cN} = \frac{1}{\alpha T_{\Sigma,N}} \tag{19}$$

with a phase margin of

$$\phi_{RN} = 2\tan^{-1}\alpha - 90° \ . \tag{20}$$

Since the controller design was based on the assumption of a simplified delay behaviour (17), deviations are to be expected for the realistic behaviour according to (14). As a matter of fact, if dead times are more dominant than delay times, which applies to the case of small ratios $T_{FN}/T_{\Sigma,i}$, the actual crossover frequency tends to be a bit higher than indicated in (19), while the actual phase margin is smaller than in (20). The Bode plots in Fig. 8 shall illustrate this situation of magnitude and phase close to the gain crossover. Again, the normalized frequency Ω according to (5) was used. It can be concluded that the stability becomes more critical, if the control loops are designed with high dynamic (high γ for current and low α for speed control).

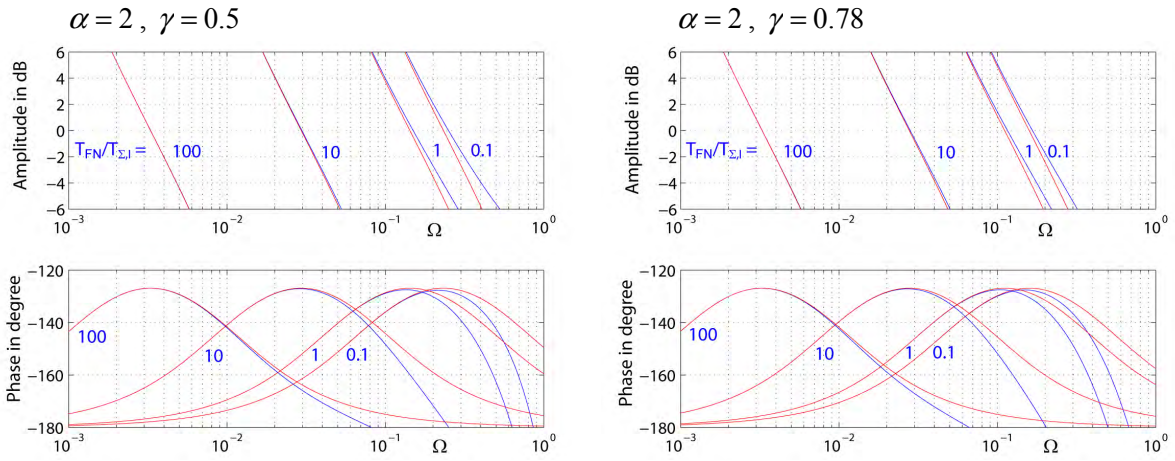

Fig. 7: Loop transfer function $F_{ON}(j\Omega)$ for various ratios $T_{FN}/T_{\Sigma,I}$, $T_{TN} = 0$,
blue curves: exact calculation, red curves: approximation with effective delay time $T_{\Sigma,N}$

Though most desirable, an explicit formula for the resulting bandwidth of the closed-loop transfer behaviour (15) cannot be found. Therefore, the calculation has been carried out numerically for different cases of speed control dead times T_{TN}, speed measurement filter constants T_{FN}, and control design parameters γ and α. In Fig. 8, the magnitude bandwidth $\Omega_{BA,N}$ is depicted with solid lines, the phase bandwid

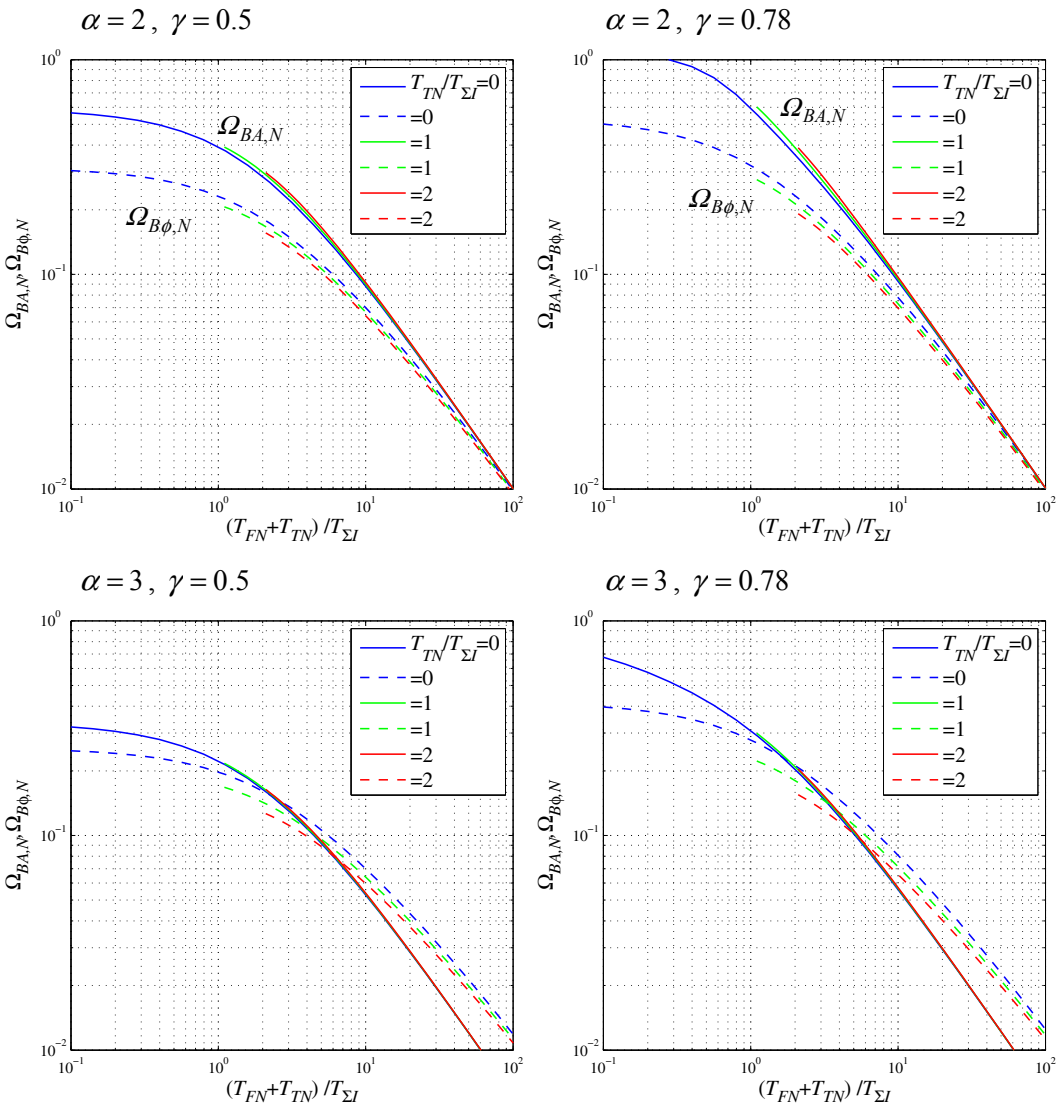

Fig. 8: Speed control bandwidth for various parameter conditions,
solid lines: magnitude bandwidth $\Omega_{BA,N}$, dashed lines: phase bandwidth $\Omega_{B\phi,N}$

As the diagrams show, magnitude and phase bandwidths $\Omega_{BA,N}$ and $\Omega_{B\phi,N}$ of approximately up to 1.0 and 0.5, respectively, can be achieved. These values are relatively high when comparing them to the previously discussed current control bandwidths which are only a little larger (Fig. 2). This circumstance is not realistic, however, as it implies that no additional dead time and speed filter are present. No additional computational delays can only be assumed in case of a speed control algorithm being processed with the same sampling frequency and within the same time slot as the current control. However, in many cases, the speed control is being processed only every second step of the current control resulting in a dead time $T_{TN} = 0.5\,T_c$ (cp. Fig. 3, cases a and b). In case the speed signal is not directly provided by the sensor, but has to be derived from the position signal by numerical differentiation, the dead time is even higher. In many cases, $T_{TN} = 1.0 \cdot T_{\Sigma,I}$ is a realistic assumption. Not surprisingly, the bandwidth is decreasing rapidly with increasing T_{TN} or T_{FN}. Whether a dead time T_{TN} or a delay T_{FN} contributes to the sum $T_{TN} + T_{FN}$ is rather secondary, as also indicated by the figures. Nevertheless, the overall situation remains similar to that of the current

control, i.e.: If a high speed control bandwidth is to be achieved, filter time constants and additional computational dead time need to be set to their smallest possible values. A high speed sensor quality and the related low demands on the post processing of the speed signal is of major significance in this context. Finally, by applying a dynamic controller tuning, like $\gamma = 0.78$, $\alpha = 2$, combined with a small additional delay of $(T_{TN} + T_{FN})/T_{\Sigma,I} = 1$, magnitude and phase bandwidths $\Omega_{BA,N} \approx 0.6$ and $\Omega_{B\phi,N} \approx 0.3$, respectively, become possible.

For example, assuming a given switching frequency of $f_s = 16$ kHz and a sampling strategy according to Fig. 3, case b, leading to $T_{\Sigma,I} = 1/f_s = 62.5\,\mu s$, the absolute speed control bandwidths result in $f_{BA,N} \approx f_s \cdot 0.6/2\pi \approx f_s/10 \approx 1.5\,\text{kHz}$ and $f_{B\phi,N} \approx f_s \cdot 0.3/2\pi \approx f_s/20 \approx 0.7\,\text{kHz}$.

The above design considerations have been verified by measurements, as shown in Fig. 9. The plots provide comparisc (16), (17). While the exact modelling (dark green lines) corresponds to the measured frequency responses quite well, the simplified model (blue lines) with effective delay time leads to major deviations, as already expected earlier.

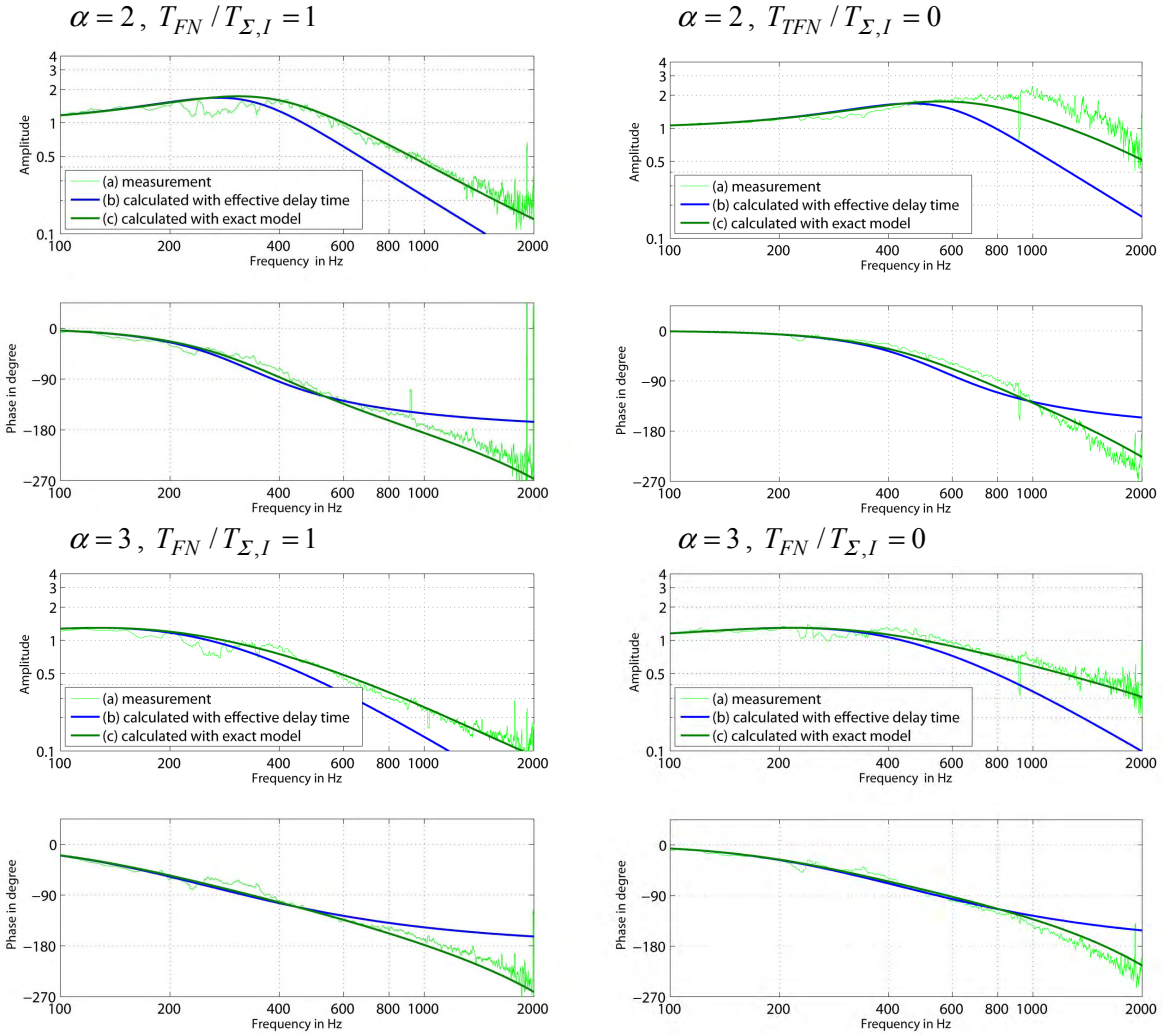

Fig. 9: Comparison of measured and computed speed control frequency responses, constant parameters for all diagrams: $\gamma = 0.78$, $T_{TN}/T_{\Sigma,I} = 1$

$\alpha = 2$, $T_{FN}/T_{\Sigma,I} = 0$ $\alpha = 3$, $T_{FN}/T_{\Sigma,I} = 0$

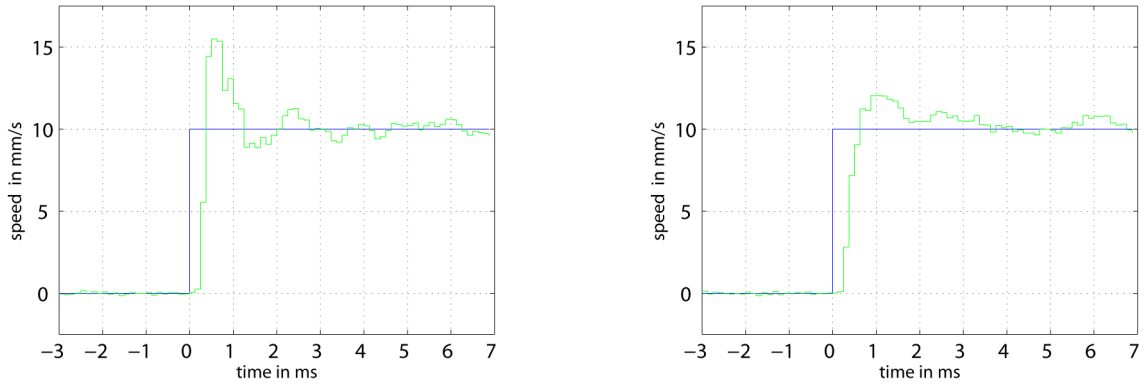

Fig. 10: Step responses of speed control, $\gamma = 0.78$, $T_{TN} / T_{\Sigma,I} = 1$

Fig. 10 shows measurements of step responses of the speed control with $T_{\Sigma,I} = 62.5\,\mu s$ and the other design parameters as specified. The reference value is reached within 2 to 4 sampling intervals of the speed control.

6 Conclusions

It has been shown in detail, how the maximum bandwidths of servo drives depend on switching and sampling frequencies, sampling strategy, filter time constants, and the control design parameters. For that purpose, the control loops have been modelled relying on a combination of delay and dead time elements. This modelling concept has been accurately validated by measurements that have been carried out with an ironless linear motor drive of small inertia as applied for production machines with highest dynamics.

As a result, speed control bandwidths within the range of 1/10 to 1/20 of the switching frequency can be achieved with a standard control design approach. Prerequisites are, however, an optimized sampling and control processing task timing as well as the dispensability of speed measurement smoothing filters. Suboptimal task timing or low-resolution position encoders that require smoothing filters with large time constants would significantly degrade the controller's dynamic performance and thus reduce the maximum achievable bandwidth.

In this context, the decisive parameters in order to aim for higher bandwidths are the effective control dead times. These can be reduced even further, e.g. by utilization of fast controller hardware as FPGA, possibly combined with oversampling technique [12], even if the switching frequency is kept constant.

References

[1] W. Leonhard: *Control of Electric Drives*, 3rd edition, Springer, 2001
[2] Schröder, D.: *Elektrische Antriebe – Regelung von Antriebssystemen*, Springer, 2nd edition, 2001
[3] Zäh, M.; Brandenburg, G.: *Das erweiterte Dämpfungsoptimum*, Automatisierungstechnik at 35, H. 7, 1987, pp. 275-283
[4] S. Beineke, A. Bähr: *Observer-Based Speed Estimation for Linear Motor Control*; PCIM, Nuremberg, 2006
[5] A. Bähr, S. Beineke: *Mechanical Resonance Damping in an Industrial Servo Drive*, EPE 2007, Aalborg
[6] S. Beineke, L. Hebing, A. Bünte: *High-Speed Drive with Three-Level Inverter for Vacuum Pumps, Laser Cooling and High-Speed Cutting*, EPE 2003, Toulouse
[7] L. Kucera: *Optimale Architektur zur Regelung hochdynamischer und Resonanzbehafteter Antriebe*, SPS/DRIVES 2006, Nuremberg, pp. 455 -462
[8] H. Schmirgel, J. O. Krah, R. Berger: *Delay Time Compensation in the Current Control Loop of Servo Drives – Higher Bandwidth at no Trade-off*, PCIM, Nuremberg, 2006, pp. 541-546
[9] L. Springob: *Synchron-Servoantrieb mit hoher Rundlaufgüte und Selbstinbetriebnahmefunktion*, Diss., Wuppertal, 1994
[10] S. Beineke, A. Bähr: *High Performance Motion Control of Linear Motor Drives*, EPE 2005, Dresden
[11] S. Beineke, A. Bähr, F. Mink, R. Nalepa: *Regelung von Synchronmotoren mit Kompensation von Sättigungseffekten*, SPS/DRIVES 2008, Nuremberg
[12] S. Mathapati, J. Böcker, *Implementation of Dynamically Reconfigurable Control Structures on a Single FPGA Platform*, EPE 2007, Aalborg, Denmark